Electron energy loss in multilayered slabs. II. Parallel incidence

1995 J. Phys.: Condens. Matter 7 3389

(http://iopscience.iop.org/0953-8984/7/18/004)

J. Phys.: Condens. Matter 7 (1995) 3389–3403. Printed in the UK

Electron energy loss in multilayered slabs: II. Parallel incidence

J P R Bolton and M Chen

Physics Department, The Open University, Walton Hall, Milton Keynes MK7 6AA, UK

Received 28 July 1994

Abstract. This paper develops the dielectric theory of energy loss, including retardation effects, for electrons travelling parallel to the interfaces of a stratified slab. A transfer matrix recurrence relation is introduced to implement the boundary conditions at surfaces and interfaces. This recurrence relation is solved exactly to provide closed formulae for the Hertz vector, the dispersion relation and the energy-loss probability, valid for any position of the beam and any number of layers. The non-retarded limits of these expressions are also examined and compared with the results of a simpler calculation based directly on Poisson's equation. Our final results are illustrated by numerical calculations applied to Al/Al_2O_3 multilayers and a InSb/GaP bilayer.

1. Introduction

In a companion paper (referred to here as paper I) we developed the dielectric theory of electron energy loss for normal incidence on a multilayered slab, obtaining compact expressions for the Hertz vector, the dispersion relation and the energy-loss spectrum [1]. In this paper, we carry out similar calculations for parallel incidence. In some respects, this is a more complicated task than for normal incidence because we now have to deal with a 4×4 transfer matrix and allow for the beam to be in any layer of the slab or in either of the two external regions. In compensation, however, the source terms do not vary from layer to layer and the work done by the beam can be calculated without summing over layers. So far as possible, we will adopt the notation of paper I. In particular, we will reuse the variables σ, f_j, q_j, h^{σ}_{ji}, C_{ji}, D_{ji}, E_{ji} and F_{ji}, and make extensive use of dispersion brackets. The reader is referred to paper I for definitions of these terms.

Parallel incidence has been extensively studied for single interfaces and homogeneous slabs. Howie and co-workers [2, 3, 4] have calculated the energy losses in the neighbourhood of an interface between two bulk media. They showed [4] that there can be significant differences between spectra calculated using the retarded and electrostatic formalisms, especially if the beam is near the interface. Parker [5, 6] has extended the retarded calculations to a single slab, obtaining separate formulae for internal and external beams. In this paper we shall consider parallel incidence on a multilayered slab composed of any finite number of layers. The aim is to obtain a single unified formula for the energy-loss spectrum that applies no matter where the beam is or how many layers the slab contains.

The paper is organized as follows. In section 2 we state the problem and develop a transfer matrix recurrence relation for the Hertz vector which incorporates the relevant boundary conditions. Section 3 gives a useful result for products of transfer matrices, needed for the remainder of our analysis. In sections 4 and 5 we obtain closed formulae for

0953-8984/95/183389+15$19.50

the dispersion relation, the Hertz vector and the semiclassical energy-loss spectrum. The symmetries of these results are examined in section 6, and special cases compared with previously established formulae. In particular, we examine the non-retarded limit of our answers and show that they agree with the results of a direct calculation based on Poisson's equation (included in an appendix). Section 7 illustrates some consequences of the theory by carrying out numerical calculations for Al/Al_2O_3 multilayers and a semiconductor bilayer. Finally, section 8 summarizes our findings and provides an outlook to future work.

As in paper I, we can only give an outline of our derivations here; readers interested in following through the proofs will find further details in [7] and [8]. On the other hand, readers who wish only to use our final results may wish to concentrate on equations (12), (13), (19) and (20), bearing in mind that section 3 of paper I and section 3 of this paper contain definitions that are needed to interpret these formulae.

2. The transfer matrix recurrence relation

We consider a stratified slab which extends to infinity in the x- and y-directions and from $z = 0$ to $z = a$ (figure 1). The slab comprises n layers, labelled $1, \ldots, n$. The jth layer lies between z_{j-1} and z_j, has thickness $a_j = z_j - z_{j-1}$ and local dielectric function $\epsilon_j(\omega)$. The external regions, which need not be vacua, are labelled 0 and $n+1$ and extend from $z_{-1} = -\infty$ to $z_0 = 0$ and from $z_n = a$ to $z_{n+1} = +\infty$. The incident beam is assumed to travel at constant speed v parallel to the x-axis and to occupy region m, where $0 \leqslant m \leqslant n+1$. We investigate the effects of a particle in the beam of charge Q, with coordinates $x = vt$, $y = 0$ and $z = z_b$. Primes are used to distinguish between the subregions on either side of the beam: m' lies between z_{m-1} and z_b, while m'' lies between z_b and z_m.

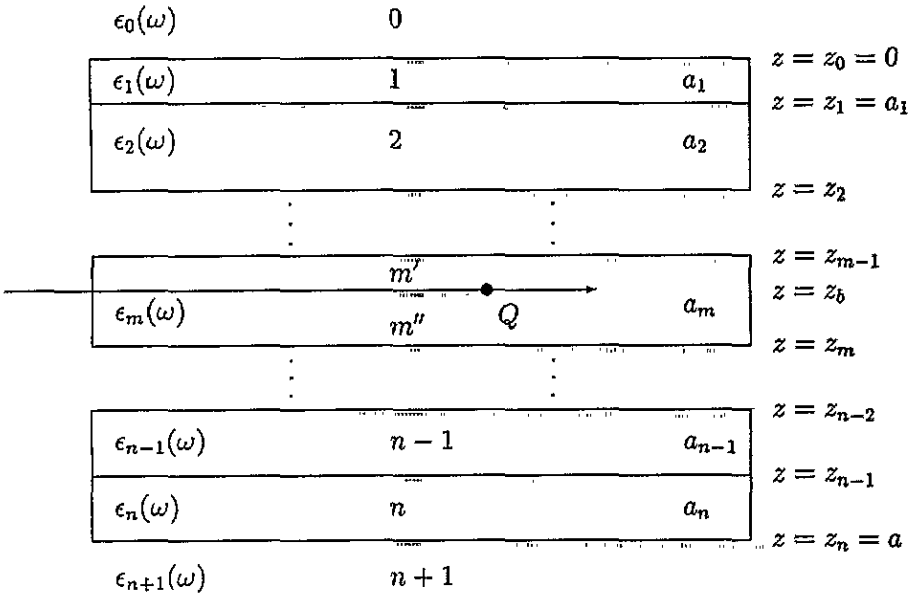

Figure 1. Multilayer geometry for parallel incidence.

To apply the semiclassical dielectric formalism we must first solve Maxwell's equations which are conveniently expressed in terms of the Hertz vector. We Fourier transform from

(x, y, z, t) to (k_x, k_y, z, ω) and write the Fourier-transformed Hertz vector in region j as

$$\mathbf{\Pi}^{(j)}(k_x, k_y, z, \omega) = \hat{\mathbf{\Pi}}^{(j)}\,\delta(k_x v - \omega)$$

where $\hat{\mathbf{\Pi}}_j$ is a continuous vector function whose x-component has a discontinuous derivative at the z-coordinate of the beam:

$$\hat{\Pi}_x^{(m'')}\Big|_{z_b^+} = \hat{\Pi}_x^{(m')}\Big|_{z_b^-} \qquad \text{and} \qquad \frac{\mathrm{d}\hat{\Pi}_x^{(m'')}}{\mathrm{d}z}\bigg|_{z_b^+} - \frac{\mathrm{d}\hat{\Pi}_x^{(m')}}{\mathrm{d}z}\bigg|_{z_b^-} = 2q_m\lambda_m$$

with

$$\lambda_m = \frac{\pi Q v}{\mathrm{i}\omega\epsilon_0}\frac{1}{q_m\epsilon_m}.$$

Then Maxwell's equations are satisfied by taking

$$\hat{\mathbf{\Pi}}^{(j)} = \left(A_j^+ \mathrm{e}^{q_j z} + A_j^- \mathrm{e}^{-q_j z},\ 0,\ B_j^+ \mathrm{e}^{q_j z} + B_j^- \mathrm{e}^{-q_j z}\right)^{\mathrm{T}}$$

where the coefficients A_j^σ and B_j^σ depend on ω, $k_x = \omega/v$, k_y and, of course, on the region j and the beam region m. The discontinuity in slope at $z = z_b$ is dealt with by allowing the coefficients $A_{m'}^\sigma$ in subregion m' to differ from the coefficients $A_{m''}^\sigma$ in subregion m''. Since the boundary conditions at infinity require four of the coefficients to vanish, there remain $4n + 6$ undetermined coefficients. These coefficients can be found by supplementing the $4n + 4$ linear equations that describe the continuity of E_x, E_y, H_x and H_y at the $n + 1$ interfaces with the two equations that describe the continuity of $\hat{\Pi}_x$ and the discontinuity of $\mathrm{d}\hat{\Pi}_x/\mathrm{d}z$ at $z = z_b$. In principle, it is possible to solve this system of $4n+6$ equations directly using computer algebra. Our early work followed this direct approach and gave results for a single slab consistent with [5]. In practice, however, such calculations soon become unwieldy and it is far better to describe the boundary conditions in terms of a transfer matrix recurrence relation. In order to express this recurrence relation in the simplest possible form we rescale the Hertz vector coefficients as follows:

$$\alpha_j^\sigma = A_j^\sigma \mathrm{e}^{\sigma q_j z_{j-1}}/\lambda_m \qquad \text{with } \alpha_0^\sigma = A_0^\sigma/\lambda_m$$

$$\beta_j^\sigma = B_j^\sigma \mathrm{e}^{\sigma q_j z_{j-1}}/(\mathrm{i}k_x\lambda_m) \qquad \text{with } \beta_0^\sigma = B_0^\sigma/(\mathrm{i}k_x\lambda_m)$$

and then define the **coefficient vectors**

$$\boldsymbol{\alpha}_j = \left(\alpha_j^+,\ \alpha_j^-\right)^{\mathrm{T}}$$

$$\boldsymbol{\beta}_j = \left(\beta_j^+,\ \beta_j^-\right)^{\mathrm{T}}$$

$$\boldsymbol{C}_j = \left(\alpha_j^+,\ \alpha_j^-,\ \beta_j^+,\ \beta_j^-\right)^{\mathrm{T}}.$$

As in the normal calculation, we use the variables $f_j = \mathrm{e}^{q_j a_j}$ (with $f_0 = f_{n+1} = 1$) and $h_{ij}^\sigma = q_i\epsilon_j + \sigma q_j\epsilon_i$. In the case of parallel incidence, it is also convenient to introduce the variable

$$\tilde{h}_{ij}^\sigma = q_i + \sigma q_j. \tag{1}$$

Finally, we define the **source vector**

$$\boldsymbol{G}_m = \left(g_m^-,\ -g_m^+,\ 0,\ 0\right)^{\mathrm{T}}$$

where

$$g_j^\sigma = \mathrm{e}^{\sigma q_j (z_b - z_{j-1})} \qquad \text{with } g_0^\sigma = \mathrm{e}^{\sigma q_0 z_b}.$$

The boundary conditions at the interface between jth and $(j+1)$th regions (or subregions) then lead to the recurrence relation

$$\boxed{\boldsymbol{C}_{j+1} = \mathbf{T}^{(j+1,j)}(\boldsymbol{C}_j + \delta_{jm'}\boldsymbol{G}_m)} \tag{2}$$

where the 4×4 **transfer matrix** is given by

$$\mathbf{T}^{(j+1,j)} = \frac{1}{h^+_{j+1,j+1} f_j} \begin{pmatrix} \epsilon_j \begin{pmatrix} \tilde{h}^+_{j+1,j} f_j^2 & \tilde{h}^-_{j+1,j} \\ \tilde{h}^-_{j+1,j} f_j^2 & \tilde{h}^+_{j+1,j} \end{pmatrix} & \begin{pmatrix} 0 & 0 \\ 0 & 0 \end{pmatrix} \\ (\epsilon_{j+1} - \epsilon_j) \begin{pmatrix} f_j^2 & 1 \\ -f_j^2 & -1 \end{pmatrix} & \begin{pmatrix} h^+_{j+1,j} f_j^2 & h^-_{j+1,j} \\ h^-_{j+1,j} f_j^2 & h^+_{j+1,j} \end{pmatrix} \end{pmatrix} \tag{3}$$

with

$$\mathbf{T}^{(m'',m')} = \mathbf{I}.$$

It is easy to write down a formal solution to this recurrence relation:

$$\boldsymbol{C}_j = \mathbf{T}^{(j0)}\boldsymbol{C}_0 + \mathbf{T}^{(jm)}\boldsymbol{G}_m \tag{4}$$

where the **generalized transfer matrix** $\mathbf{T}^{(ji)}$ is defined by the product

$$\mathbf{T}^{(ji)} = \prod_{k=i}^{j-1} \mathbf{T}^{(k+1,k)}$$

with successive matrices ordered from right to left. In principle, this equation can be used to express the coefficients in region 0 in terms of those in region $n+1$. The boundary conditions at infinity then give

$$T_{11}^{(n+1,0)}\alpha_0^+ + T_{11}^{(n+1,m)}g_m^- - T_{12}^{(n+1,m)}g_m^+ = 0 \tag{5}$$

$$T_{31}^{(n+1,0)}\alpha_0^+ + T_{33}^{(n+1,0)}\beta_0^+ + T_{31}^{(n+1,m)}g_m^- - T_{32}^{(n+1,m)}g_m^+ = 0 \tag{6}$$

allowing us to determine the coefficients in region 0. Equations (2) or (4) then generate all the other coefficients. Such a procedure can be carried through numerically without difficulty but this approach offers little insight into the nature of the solutions or their relationship to previously derived results for bulk, single interfaces and single slabs. As in the case of normal incidence we therefore prefer to proceed analytically, with the aim of obtaining closed formulae for the quantities of interest.

3. The generalized transfer matrix

An important step in our solution is to find a compact expression for the generalized transfer matrix in terms of dispersion brackets. We will reuse the dispersion brackets $[C_{ji}]$, $[D_{ji}]$, $[E_{ji}]$ and $[F_{ji}]$ of paper I. Also here, and throughout this paper, we use a convenient shorthand: for any quantity X, we extend the tilde notation of equation (1), so $\tilde{X}$ is defined by replacing each h^σ_{ji} in X by the corresponding variable $\tilde{h}^\sigma_{ji}$. For example,

$$[\tilde{C}_{21}] = \tilde{h}^+_{32} f_2^2 \tilde{h}^+_{21} f_1^2 + \tilde{h}^-_{32}\tilde{h}^-_{21} f_1^2 = (q_3+q_2) f_2^2 (q_2+q_1) f_1^2 + (q_3-q_2)(q_2-q_1) f_1^2.$$

Using this notation, we find that the generalized transfer matrix has a block triangular form:

$$\mathbf{T}^{(j+1,i)} = \frac{1}{\kappa_{ij}} \begin{pmatrix} \eta_{ij}\tilde{\boldsymbol{\tau}}^{(j+1,i)} & \mathbf{0} \\ \boldsymbol{\theta}^{(j+1,i)} & \boldsymbol{\tau}^{(j+1,i)} \end{pmatrix} \tag{7}$$

where

$$\kappa_{ij} = \prod_{k=i}^{j} h^{+}_{k+1,k+1} f_k \tag{8}$$

$$\eta_{ij} = \prod_{k=i}^{j} \epsilon_k \tag{9}$$

and, as in paper I,

$$\tau^{(j+1,i)} = \begin{pmatrix} [C_{ji}] & [D_{ji}] \\ [E_{ji}] & [F_{ji}] \end{pmatrix}. \tag{10}$$

The matrix $\theta^{(j+1,i)}$ is more troublesome. In our early work ([7]) we obtained a closed-form expression for $\theta^{(j+1,i)}$ which involved complicated sums over many different dispersion brackets. Recently, however, we have discovered a much simpler result:

$$k^2\theta^{(j+1,i)} = q_i \begin{pmatrix} [C_{ji}] & -[D_{ji}] \\ [E_{ji}] & -[F_{ji}] \end{pmatrix} - q_{j+1}\eta_{ij} \begin{pmatrix} [\tilde{C}_{ji}] & [\tilde{D}_{ji}] \\ -[\tilde{E}_{ji}] & -[\tilde{F}_{ji}] \end{pmatrix}. \tag{11}$$

This identity (proved in [8]) will allow us to calculate many quantities of physical interest.

4. The dispersion relation

Starting from equations (5) and (6), with the source terms set equal to zero, we obtain the dispersion relation

$$T_{11}^{(n+1,0)} T_{33}^{(n+1,0)} = 0.$$

Equations (7) and (10) then allow us to write this dispersion relation in the explicit form

$$\boxed{[C_{n0}][\tilde{C}_{n0}] = 0.} \tag{12}$$

The solutions are of two types. We have proved that the $[C_{n0}] = 0$ solutions are TM modes, with $H_z = 0$ everywhere, while the $[\tilde{C}_{n0}] = 0$ solutions are TE modes, with $E_z = 0$ everywhere [8]. Both types of mode are divergenceless ($\nabla \cdot \boldsymbol{E} = 0$). However, whereas the TE interface modes are transverse (with $k_x E_x + k_y E_y = 0$), the TM interface modes are *not* transverse and have $E_x/E_y = k_x/k_y$. Comparison with paper I shows that the TE modes are new: they are not excited by normal incidence but, at this stage, cannot be ruled out for parallel incidence. In section 7 we will revisit this point and show that the dispersion curves of the TE modes are restricted to regions of k–ω space where they are difficult to excite, even in the case of parallel incidence. The TM modes will continue to be of major interest.

For symmetrical slabs with $2j+1$ layers, the dispersion relation can be further factorized (cf paper I) to give

$$\boxed{(L^{+}_{j0}L^{-}_{j0})(\tilde{L}^{+}_{j0}\tilde{L}^{-}_{j0}) = 0} \tag{13}$$

where

$$L^{\sigma}_{j0} = [C_{j0}]\, f_{j+1} + \sigma\, [E_{j0}]$$

and, for both TM and TE modes, $+$ superscripts label solutions with a symmetric charge distribution and $-$ superscripts label solutions with an antisymmetric charge distribution.

Special cases of our dispersion relation agree with established results for low values of n. For example, in the case of a single slab surrounded by a homogeneous medium, equation (13) can be used with $j = 0$ to obtain

$$\left\{(q_0\epsilon_1 + q_1\epsilon_0)^2 f_1^2 - (q_0\epsilon_1 - q_1\epsilon_0)^2\right\}\left\{(q_0 + q_1)^2 f_1^2 - (q_0 - q_1)^2\right\} = 0.$$

In this case, the solutions split into the TM modes

$$\frac{q_0\epsilon_1 + q_1\epsilon_0}{q_0\epsilon_1 - q_1\epsilon_0} = \pm e^{-q_1 a_1}$$

and the TE modes

$$\frac{q_0 + q_1}{q_0 - q_1} = \pm e^{-q_1 a_1}$$

previously given in [9] and [10].

Also, substituting $n = 0$ in equation (12) gives the dispersion relation

$$(q_1\epsilon_0 + q_0\epsilon_1)(q_1 + q_0) = 0$$

which is again of the expected form for a system with $n + 1$ interfaces (a single interface in this case). Equations (12) and (13) provide a natural generalization of these well-known results to the more complicated geometry of multilayers.

5. The Hertz vector and energy loss

Before stating our solutions for the Hertz vector, we need to to introduce some new variables:

$$\gamma_{ji}^{\sigma} = \left[C_{ji}\right] g_i^- + \sigma\left[D_{ji}\right] g_i^+$$

$$\zeta_{ji}^{\sigma} = \left[C_{ji}\right] g_{j+1}^+ + \sigma\left[E_{ji}\right] g_{j+1}^-$$

and

$$\rho_{ij} = \prod_{k=i}^{j}(2q_k f_k).$$

In terms of these variables, and using equations (4), (5) and (6), together with our expression for the generalized transfer matrix, we find that [8], for regions *before* the beam layer (i.e for $j \leqslant m'$),

$$\begin{pmatrix}\alpha_j^+\\ \alpha_j^-\end{pmatrix} = -\frac{q_m\epsilon_m}{q_j\epsilon_j}\rho_{j,m-1}\frac{\widetilde{\gamma}_{nm}^-}{\left[\widetilde{C}_{n0}\right]}\begin{pmatrix}\left[\widetilde{C}_{j-1,0}\right]\\ \left[\widetilde{E}_{j-1,0}\right]\end{pmatrix} \tag{14}$$

and

$$\begin{pmatrix}\beta_j^+\\ \beta_j^-\end{pmatrix} = \frac{\kappa_{j,m-1}}{k^2}\left\{\frac{q_j\widetilde{\gamma}_{nm}^-}{\eta_{j,m-1}\left[\widetilde{C}_{n0}\right]}\begin{pmatrix}\left[\widetilde{C}_{j-1,0}\right]\\ -\left[\widetilde{E}_{j-1,0}\right]\end{pmatrix} - \frac{q_m\gamma_{nm}^+}{\left[C_{n0}\right]}\begin{pmatrix}\left[C_{j-1,0}\right]\\ \left[E_{j-1,0}\right]\end{pmatrix}\right\}. \tag{15}$$

Similarly, for regions *beyond* the beam layer (i.e. for $j \geqslant m''$) we obtain

$$\begin{pmatrix}\alpha_j^+\\ \alpha_j^-\end{pmatrix} = -\frac{\epsilon_m}{\epsilon_j}\rho_{m,j-1}\frac{1}{\left[\widetilde{C}_{n0}\right]}\widetilde{\zeta}_{m-1,0}^+\begin{pmatrix}-\left[\widetilde{D}_{nj}\right]\\ \left[\widetilde{C}_{nj}\right]\end{pmatrix} \tag{16}$$

and

$$\begin{pmatrix}\beta_j^+\\ \beta_j^-\end{pmatrix} = -\frac{\kappa_{m,j-1}}{k^2}\frac{q_m\epsilon_m}{q_j\epsilon_j}\left\{\frac{q_j\widetilde{\zeta}_{m-1,0}^+}{\eta_{m+1,j}\left[\widetilde{C}_{n0}\right]}\begin{pmatrix}\left[\widetilde{D}_{nj}\right]\\ \left[\widetilde{C}_{nj}\right]\end{pmatrix} - \frac{q_m\zeta_{m-1,0}^-}{\left[C_{n0}\right]}\begin{pmatrix}-\left[D_{nj}\right]\\ \left[C_{nj}\right]\end{pmatrix}\right\}. \tag{17}$$

These explicit solutions for the Hertz vector lead to a closed-form semiclassical expression for the energy-loss spectrum. This is obtained by calculating the work done on the incoming electron by the electric field created by its polarized surroundings. The semiclassical energy-loss probability then follows by expressing the total energy loss in terms of the transfer of individual quanta of energy $\hbar\omega$. A straightforward calculation shows that for an n-layered slab, with the beam in region m, the energy-loss probability is described by the function

$$\frac{\mathrm{d}^3P}{\mathrm{d}(\hbar\omega)\,\mathrm{d}k_y\,\mathrm{d}x} = \frac{Q^2}{2\pi^2\varepsilon_0\hbar^2v^2}\mathrm{Im}\left\{\chi_m^{(n)}\right\}_{k_x\to\omega/v}$$

where

$$\chi_m^{(n)} = \frac{1}{q_m\epsilon_m}\sum_{\sigma=\pm}\left\{(1-\epsilon_m v^2/c^2)\alpha_m^\sigma g_m^\sigma + q_m\sigma\beta_m^\sigma g_m^\sigma\right\}. \tag{18}$$

Here, the normalization has been chosen in such a way that the work done per unit path length is

$$\frac{\mathrm{d}W}{\mathrm{d}x} \equiv \int_0^\infty \mathrm{d}(\hbar\omega)\,\hbar\omega\frac{\mathrm{d}I(\hbar\omega)}{\mathrm{d}x} = \int_0^\infty \mathrm{d}(\hbar\omega)\,\hbar\omega\int_0^{k_c}\mathrm{d}k_y\,\frac{\mathrm{d}^3P}{\mathrm{d}(\hbar\omega)\,\mathrm{d}k_y\,\mathrm{d}x}$$

where k_c is an appropriate wavevector cut-off (see paper I) and $\mathrm{d}I(\hbar\omega)/\mathrm{d}x$ is the scattering probability per unit path length, per unit energy range.

It makes no difference, in equation (18), whether one chooses to use the coefficients in the m'-subregion (equations (14) and (15)) or the coefficients in the m''-subregion (equations (16) and (17)). Whichever choice is made, our solution for the Hertz vector leads to the following explicit expression for the energy-loss function:

$$\boxed{\chi_m^{(n)} = \frac{1}{q_m\epsilon_m k^2}\left\{\epsilon_m k_y^2\frac{v^2}{c^2}\frac{\tilde{\gamma}_{nm}^-\tilde{\zeta}_{m-1,0}^+}{[\tilde{C}_{n0}]} - q_m^2\frac{\gamma_{nm}^+\zeta_{m-1,0}^-}{[C_{n0}]}\right\}.} \tag{19}$$

This equation is the main result of our analysis. It provides a remarkably simple formula for the semiclassical energy-loss spectrum, which is valid for all choices of beam region m, beam position z_b, number of layers n, layer thicknesses ($\{a_j\}$) and local dielectric functions ($\{\epsilon_j\}$). The variable ω in equation (19) is, of course, real, while the dispersion relations $[C_{n0}] = 0$ and $[\tilde{C}_{n0}] = 0$ are in general only satisfied for complex frequencies. Nevertheless, it is clear from equations (19) and (12) that the real frequencies for which the dispersion relation is *close* to to being satisfied (over a wide range of attainable k-values) are likely to be those for which there is a high probability of energy loss.

Unlike the case of normal incidence, it does not seem to be possible to express equation (19) as a quadratic form in the variables $(\epsilon_{k+1} - \epsilon_k)$. It is possible to re-express $\chi_m^{(n)}$ as a sum of terms that are *linear* in $(\epsilon_{k+1} - \epsilon_k)$; however, the resulting expression is much more complicated than equation (19) and appears to offer no advantages, so discussion of this representation is confined to [7] and [8].

6. Symmetries and special cases

In this section we establish some symmetry properties of equation (19), explore special cases and examine the non-retarded (electrostatic) limit. All these may be regarded as checks of our result.

6.1. Symmetries

As in paper I, we introduce five operators:

(i) $\hat{\mathcal{T}}_v$ reverses the sign of v;

(ii) $\hat{\mathcal{T}}_\omega$ reverses the sign of ω;

(iii) $\hat{\mathcal{P}}_k$ reverses the sign of q_k but leaves q_j unchanged for $j \neq k$;

(iv) $\hat{\mathcal{S}}$ reverses the labelling of the regions so that $k \to n+1-k$;

(v) $\hat{\mathcal{J}}_{k,k+1}$ causes two neighbouring regions k and $k+1$ to coalesce.

Inspection of equation (19) immediately confirms that

$$\hat{\mathcal{T}}_\omega(\chi_m^{(n)}) = \chi_m^{(n)*} \qquad \text{and} \qquad \hat{\mathcal{T}}_v(\chi_m^{(n)}) = \chi_m^{(n)}.$$

The transformation $\hat{\mathcal{P}}_k$ has a non-trivial effect on the individual terms of equation (19). For example,

$$\hat{\mathcal{P}}_k(\zeta_{m-1,0}^{\sigma}) = \begin{cases} -\zeta_{m-1,0}^{\sigma}/f_k^2 & \text{if } 0 < k \leqslant m-1 \\ -\sigma\,\zeta_{m-1,0}^{\sigma} & \text{if } k = m \\ \zeta_{m-1,0}^{\sigma} & \text{if } k \geqslant m+1. \end{cases}$$

Nevertheless, it is possible to show that

$$\mathcal{P}_k(\chi_m^{(n)}) = \chi_m^{(n)} \qquad \text{for all } k.$$

The transformation $\hat{\mathcal{S}}$ gives

$$\hat{\mathcal{S}}(\gamma_{nm}^{\sigma}) = \zeta_{n-m,0}^{-\sigma} f_{n+1-m} \qquad \text{and} \qquad \hat{\mathcal{S}}(\zeta_{m-1,0}^{\sigma}) = \gamma_{n,n+1-m}^{-\sigma}/f_{n+1-m}.$$

When these results are substituted in equation (19), we find that

$$\hat{\mathcal{S}}(\chi_m^{(n)}) = \chi_{n+1-m}^{(n)}$$

as expected.

Finally, we can consider the effect of allowing two neighbouring regions to coalesce. This corresponds to making the replacements $\epsilon_{k+1} \to \epsilon_k$, $q_{k+1} \to q_k$ etc, $2a_k \to a_k$ and then renumbering the layers $j \to j-1$ for $j \geqslant k$. When this transformation is applied to equation (19), we obtain the anticipated result:

$$\hat{\mathcal{J}}_{k,k+1}(\chi_m^{(n)}) = \begin{cases} \chi_{m-1}^{(n-1)} & \text{if } k < m \\ \chi_m^{(n-1)} & \text{if } k > m. \end{cases}$$

6.2. Symmetrical slabs

Even if we have a slab that is symmetrical about its central layer, the energy-loss function for parallel incidence does not simplify beyond equation (19) *unless* the beam is in the middle of the central layer. This special case will now be explored.

We consider a slab of $2m-1$ layers, symmetrical about the central mth layer, with a central beam. In this case,

$$g_m^+ = f_m^{1/2} \qquad \text{and} \qquad f_{n+1-m} = f_m$$

$$\zeta_{m-1,0}^{\sigma} = (1/f_m^{1/2}) L_{m-1,0}^{\sigma} \qquad \text{and} \qquad \gamma_{nm}^{\sigma} = f_m^{1/2} L_{m-1,0}^{-\sigma}.$$

Recalling equation (13), the energy-loss function then simplifies to

$$\boxed{\chi_m^{(2m+1)} = \frac{1}{q_m \epsilon_m k^2} \left\{ \epsilon_m k_y^2 \frac{v^2}{c^2} \frac{\tilde{L}_{m-1,0}^{+}}{\tilde{L}_{m-1,0}^{-}} - q_m^2 \frac{L_{m-1,0}^{-}}{L_{m-1,0}^{+}} \right\}} \tag{20}$$

which suggests that interfacial peaks in the energy-loss spectrum may be associated with either *symmetric* TM modes or *antisymmetric* TE modes. As mentioned earlier, the TE modes are difficult to excite so, in practice, the symmetric TM modes form the dominant interfacial features in the spectrum (see section 7).

6.3. Special cases

Next, we compare our energy-loss formula with known results for parallel incidence, beginning with a single slab. On substituting $n = 1$ and $m = 0$ in equation (19) and rearranging we recover (a compact form of) Parker's formula [5] for an *external* beam:

$$\chi_0^{(1)} = \frac{1}{q_0}\left(\frac{v^2}{c^2} - \frac{1}{\epsilon_0}\right) - \frac{(g_0^+)^2}{q_0\epsilon_0 k^2}\left\{\epsilon_0 k_y^2 \frac{v^2}{c^2}\frac{[\widetilde{D}_{10}]}{[\widetilde{C}_{10}]} + q_0^2\frac{[D_{10}]}{[C_{10}]}\right\}.$$

Substituting $n = 1$ and $m = 2$ gives the same answer, but with the replacements $g_0^\sigma \leftrightarrow g_2^{-\sigma}$, $\epsilon_0 \leftrightarrow \epsilon_2$, $q_0 \leftrightarrow q_2$ (and hence $[D_{10}] \leftrightarrow -[E_{10}]$), as expected from symmetry. Moreover, substituting $n = 1$ and $m = 1$ into equation (19) gives a result consistent with Parker's formula for an *internal* beam ([5]).

Equation (19) can even be used where no slab is present. Since the number of interfaces is $n + 1$, the case of a single interface corresponds to setting $n = 0$. If we also set $m = 0$, equation (19) gives

$$\chi_0^{(0)} = \frac{1}{q_0}\left(\frac{v^2}{c^2} - \frac{1}{\epsilon_0}\right) - \frac{(g_0^+)^2}{q_0\epsilon_0 k^2}\left\{\epsilon_0 k_y^2 \frac{v^2}{c^2}\left(\frac{q_1 - q_0}{q_1 + q_0}\right) + q_0^2\left(\frac{q_1\epsilon_0 - q_0\epsilon_1}{q_1\epsilon_0 + q_0\epsilon_1}\right)\right\}$$

which agrees with the standard formula for a relativistic interface [6, 4]. Substituting $n = 0$ and $m = 1$ in equation (19) gives the same answer, but with the replacements $\epsilon_0 \leftrightarrow \epsilon_1$, $q_0 \leftrightarrow q_1$ and $g_0^\sigma \leftrightarrow g_1^{-\sigma}$, as expected from symmetry.

Finally, we can consider the case of a bulk medium with no interfaces, which corresponds to $n = -1$. Substituting $n = -1$ and $m = 0$ into equation (19) gives

$$\chi_0^{(-1)} = \frac{1}{q_0}\left(\frac{v^2}{c^2} - \frac{1}{\epsilon_0}\right)$$

which, after integrating over the azimuthal angle, gives a result equivalent to that of Landau and Lifshitz [11].

6.4. The non-retarded limit

The non-retarded limit of equation (19) is obtained by letting $v/c \to 0$ and $\omega/ck \to 0$. The result is described most conveniently in terms of the variables

$$\check{h}_{ji}^\sigma = \epsilon_j + \sigma\epsilon_i$$

$$\check{f}_j = \mathrm{e}^{ka_j} \qquad \text{with } \check{f}_0 = \check{f}_{n+1} = 1$$

$$\check{g}_m^\sigma = \mathrm{e}^{\sigma k(z_b - z_{m-1})} \qquad \text{with } \check{g}_0^\sigma = \mathrm{e}^{\sigma k z_b}.$$

We adopt a convention analogous to that previously used for the tilde accent: any quantity $\check{X}$ is defined in the same way as its cousin X, but with h_{ji}^σ, f_j and g_j^σ replaced by $\check{h}_{ji}^\sigma$, $\check{f}_j$ and $\check{g}_0^\sigma$. Using these definitions, we find that

$$\boxed{\lim_{c\to\infty} \chi_m^{(n)} = -\frac{\check{\gamma}_{nm}^- \check{\zeta}_{m-1,0}^+}{k\epsilon_m\left[\check{C}_{n0}\right]}.} \tag{21}$$

In the appendix, we carry out a direct calculation of the non-retarded energy-loss probability, using methods similar to those described in section 4, but based on Poisson's equation for the electrostatic potential. Equation (21) agrees with this electrostatic result.

7. Calculated energy-loss spectra

This section uses the (retarded) formulae developed above to calculate energy-loss spectra for a selection of model and real systems. We concentrate on two main issues: the effect of changing the number of layers and the effect of changing the position of the beam. As in the case of normal incidence, we consider incident electrons of energy 100 keV and introduce a wavevector cut-off $k_c = 15\ \text{nm}^{-1}$ in all integrals over k_y.

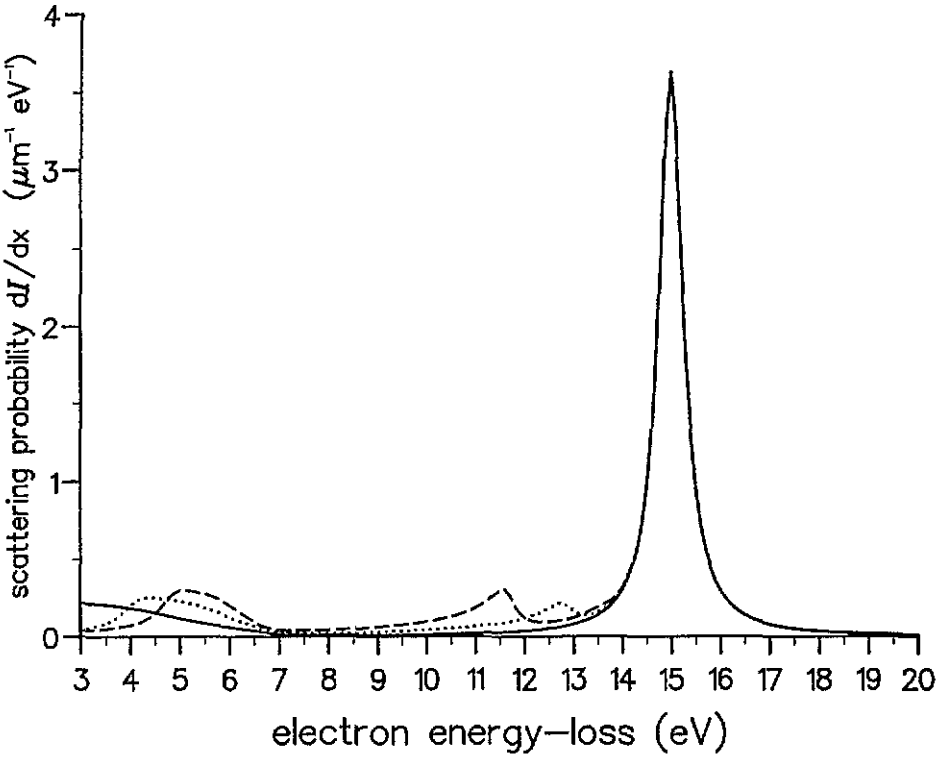

Figure 2. Scattering probability per unit path length per unit energy range, $dI(\hbar\omega)/dx$, for parallel incidence in the centre of Al/Al_2O_3 multilayers. The central layer is always Al, the outer layers Al_2O_3 and each layer is 3 nm thick. The scattering probability is shown for slabs composed of three layers (solid line), seven layers (dotted line), and eleven layers (dashed line).

Our first example discusses symmetrical multilayered slabs of Al and Al_2O_3, containing various numbers of layers. In each case, the central layer is Al and the outer layers are Al_2O_3. The dielectric functions for these materials are represented by the same models as in paper I. Figure 2 shows the scattering probability per unit path length per unit energy range for symmetrical Al/Al_2O_3 multilayers of three, seven and eleven layers. Each layer is 3 nm thick and the beam is in the middle of the central Al layer. The main loss feature in all cases is, of course, the Al bulk plasmon at 15 eV. Because of the choice of geometry and dielectric functions, there are no surface plasmons due to Al or Al_2O_3. Cherenkov radiation

is also suppressed below 15 eV because the dielectric function of Al has a negative real part in this region. The remaining peaks are associated with interfacial plasmons. They fall into two main groups: peaks below 7 eV and peaks above 10 eV. Note that the upper peak is missing in the three-layer case and the positions of the peaks shift as the number of layers increases.

Figure 3 provides more detail of our solutions by plotting $d^3P/d(\hbar\omega)\,dk_y\,dx$ against k_y and $\hbar\omega$ for the three, seven and eleven-layer slabs of figure 2. In each case, scattering by the Al plasmon produces a ridge at 15 eV. The remaining ridges are due to interface modes. We have solved the dispersion relation (equation (13)) for the systems shown in figure 3 and found that the interfacial ridges correspond closely to the dispersion curves for *symmetric* TM modes. As predicted by equation (20), the antisymmetric TM modes are not excited because the slab is symmetrical and the beam occupies an exactly central position. Our solutions to the dispersion relation show that the seven- and eleven-layer systems have symmetric TM modes at both 'low' energy (<7 eV)) and 'high' energy (>10 eV), but the three-layer system has only one symmetric TM mode, which occurs in the low-energy region (cf. [12]); this explains the missing peak in the three-layer slab. The shift in the peaks reflects the increasing complexity of mode structure that arises from coupling between different interfaces.

Figure 3 shows no trace of a contribution due to TE modes. This can again be explained in terms of the dispersion relation for these modes. Although TE modes can be found as functions of k and ω, a numerical search based on equation (12) reveals no TE modes in the region $k > \omega/v$. (This is related to the transverse nature of these modes, which prevents them from crossing the light cone $\omega = ck$.) As our energy-loss formula involves the substitution $k_x \to \omega/v$, there is no value of k_y that produces significant scattering by the TE modes.

Figure 4 shows the effect of moving the beam away from the central position in the case of the seven-layer Al/Al_2O_3 slab. This figure shows how $dI(\hbar\omega)/dx$ varies as the beam position is moved from the middle of the central Al layer to the first Al/Al_2O_3 interface. As might be expected, the structure in the interfacial modes becomes more evident as the beam approaches the interface, with both symmetric and antisymmetric TM modes being excited. However, the full structure only emerges when the beam (or part of it) is within a few Å of the interface!

Finally, we consider a semiconductor bilayer. As explained in paper I, many semiconductors have dielectric functions that are broadly similar over the energy range of interest, making it difficult to observe interfacial plasmons at semiconductor/semiconductor boundaries. In figure 5 we have deliberately chosen two semiconductors that are fairly dissimilar. The graph shows $dI(\hbar\omega)/dx$ as a function of beam position and energy loss for a two-layered slab of InSb (from 0 nm to 5 nm) and GaP (from 5 nm to 10 nm), with dielectric functions taken from [13]. The bulk plasmons for these two materials occur at 11.8 eV and 15.9 eV and surface plasmons are also visible. The main interest here, however, is the fact that an interfacial plasmon can be identified at about 13.4 eV, consistent with our feeling that parallel incidence gives the best chance of observing interfacial modes in difficult cases.

8. Conclusions and outlook

In this paper we have extended the programme of paper I to deal with parallel incidence on a multilayered slab, obtaining closed formulae for the dispersion relation and the energy-loss spectrum. The dispersion bracket algebra, introduced in the context of normal incidence, has

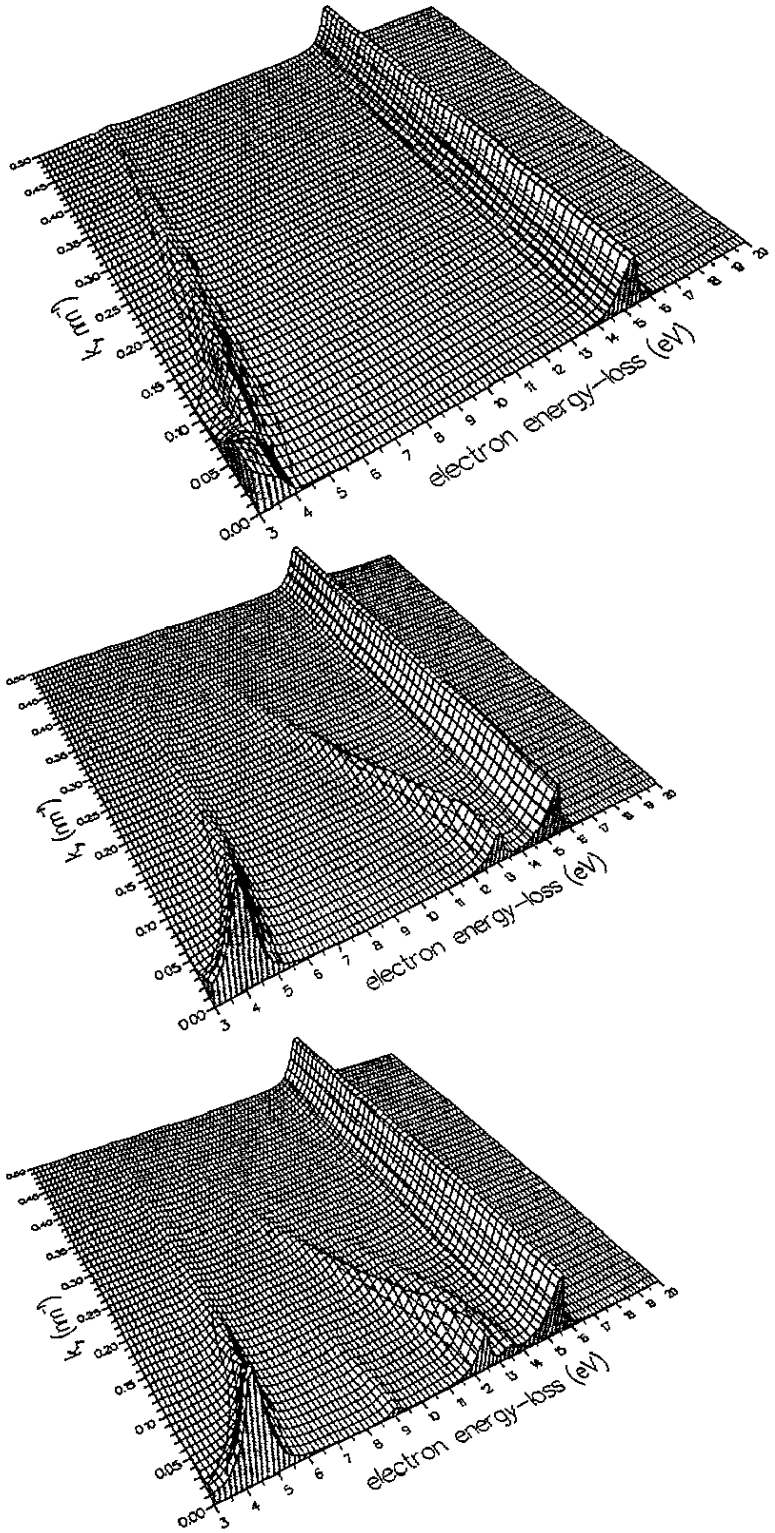

Figure 3. Three-dimensional plots of $d^3P/d(\hbar\omega)\,dk_y\,dx$ against k_y and $\hbar\omega$ for the Al/Al_2O_3 multilayers of figure 1, with the beam in the centre of the slab. From top to bottom, the plots refer to three-, seven- and eleven-layer systems.

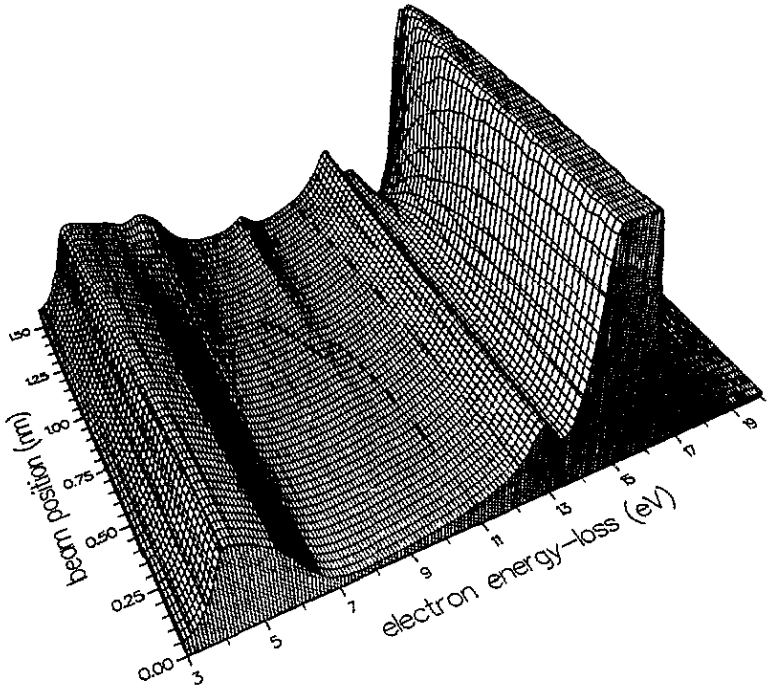

Figure 4. A three-dimensional plot of scattering probability per unit path length per unit energy range, $(\mathrm{d}I(\hbar\omega)/\mathrm{d}x)$, against energy and beam position for the seven-layer Al/Al_2O_3 slab.

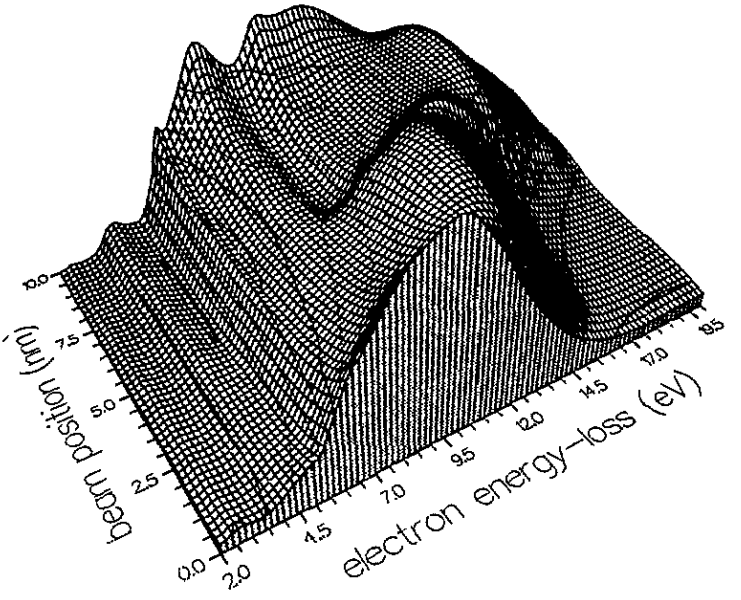

Figure 5. A three-dimensional plot of scattering probability per unit path length per unit energy range, $\mathrm{d}I(\hbar\omega)/\mathrm{d}x$, against energy and beam position for a InSb/GaP double film. InSb extends from 0 nm to 5 nm and GaP from 5 nm to 10 nm.

turned out to be valuable in the case of parallel incidence as well. Moreover, as expected, it

is easier to observe surface and interface plasmons with parallel incidence than with normal incidence. The type of calculations outlined here can be extended to other cases. We are currently using computer algebra to analyse energy loss in anisotropic slabs and in the case of oblique incidence on multilayered slabs. The oblique calculation combines the difficulties of parallel incidence (the same 4×4 transfer matrix) with those of normal incidence (source terms which vary from layer to layer and the need to sum over regions), but we hope to solve these problems in the near future.

Appendix A. The non-retarded calculation

In the electrostatic limit, the problem reduces to solving Poisson's equation subject to appropriate boundary conditions. The x, y, and t Fourier-transformed solution for the potential in the jth region can be expressed as

$$\phi_j = \hat{\phi}_j \, \delta(k_x v - \omega)$$

where

$$\hat{\phi}_j = \check{A}_j^+ \mathrm{e}^{kz} + \check{A}_j^- \mathrm{e}^{-kz} \tag{A1}$$

and, as explained previously, the accent $\check{}$ is used to distinguish non-retarded quantities from similar ones used in the normal and parallel retarded calculations. The coefficients $\check{A}_j^\sigma$ are determined from the boundary conditions at surfaces and interfaces, together with two supplementary conditions at the level of the beam:

$$\hat{\phi}_{m''}\Big|_{z_b^+} = \hat{\phi}_{m'}\Big|_{z_b^-} \qquad \text{and} \qquad \frac{\mathrm{d}\hat{\phi}_{m''}}{\mathrm{d}z}\bigg|_{z_b^+} - \frac{\mathrm{d}\hat{\phi}_{m'}}{\mathrm{d}z}\bigg|_{z_b^-} = 2k\check{\lambda}_m$$

where

$$\check{\lambda}_m = -\frac{\pi Q}{k\varepsilon_0 \epsilon_m}.$$

We rescale the coefficients $\check{A}_j^\sigma$ as follows:

$$\check{\alpha}_j^\sigma = \check{A}_j^\sigma \mathrm{e}^{\sigma k z_{j-1}} / \check{\lambda}_m \qquad \text{with } \check{\alpha}_0^\sigma = \check{A}_0^\sigma / \check{\lambda}_m.$$

Then, applying the boundary conditions at jth interface we obtain a transfer matrix recurrence relation of the form

$$\begin{pmatrix} \check{\alpha}_{j+1}^+ \\ \check{\alpha}_{j+1}^- \end{pmatrix} = \frac{1}{\check{h}_{j+1,j+1}^+ \check{f}_j} \begin{pmatrix} \check{h}_{j+1,j}^+ \check{f}_j^2 & \check{h}_{j+1,j}^- \\ \check{h}_{j+1,j}^- \check{f}_j^2 & \check{h}_{j+1,j}^+ \end{pmatrix} \begin{pmatrix} \check{\alpha}_j^+ \\ \check{\alpha}_j^- \end{pmatrix} + \delta_{jm'} \begin{pmatrix} \check{g}_m^- \\ -\check{g}_m^+ \end{pmatrix}$$

where $\check{h}_{ji}^\sigma$, $\check{f}_j$ and $\check{g}_j^\sigma$ are defined in section 6.4.

This recurrence relation leads to the dispersion relation

$$\left[\check{C}_{n0}\right] = 0$$

which agrees with the classical limit of equation (12). (There is no contribution from the TE modes in the electrostatic limit.)

By repeatedly applying the recurrence relation from external region 0 to external region $n+1$, and using the boundary conditions at infinity, we obtain $\check{\alpha}_0^+$. Then, applying the recurrence relation from region 0 to region m', we obtain the beam layer coefficients in the form

$$\begin{pmatrix} \check{\alpha}_{m'}^+ \\ \check{\alpha}_{m'}^- \end{pmatrix} = -\frac{\check{\gamma}_{nm}^-}{\left[\check{C}_{n0}\right]} \begin{pmatrix} \left[\check{C}_{m-1,0}\right] \\ \left[\check{E}_{m-1,0}\right] \end{pmatrix}.$$

The transfer matrix recurrence relation also gives the coefficients on the other side of the beam:

$$\begin{pmatrix} \check{\alpha}^{+}_{m''} \\ \check{\alpha}^{-}_{m''} \end{pmatrix} = -\frac{\check{\zeta}^{+}_{m-1,0}}{\left[\check{C}_{n0}\right]} \begin{pmatrix} -\left[\check{D}_{nm}\right] \\ \left[\check{C}_{nm}\right] \end{pmatrix}.$$

The scattering probability per unit path length can finally be expressed as

$$\frac{\mathrm{d}^3 P}{\mathrm{d}(\hbar\omega)\,\mathrm{d}k_y\,\mathrm{d}x} = \frac{Q^2}{2\pi^2\varepsilon_0\hbar^2 v^2}\mathrm{Im}\left\{\check{\chi}^{(n)}_m\right\}_{k_x\to\omega/v} \tag{A2}$$

where

$$\check{\chi}^{(n)}_m = \frac{1}{k\epsilon_m}\sum_{\sigma=\pm}\check{\alpha}^{\sigma}_{m'}\check{g}^{\sigma}_m = \frac{1}{k\epsilon_m}\sum_{\sigma=\pm}\check{\alpha}^{\sigma}_{m''}\check{g}^{\sigma}_m = -\frac{\check{\gamma}^{-}_{nm}\check{\zeta}^{+}_{m-1,0}}{k\epsilon_m\left[\check{C}_{n0}\right]} \tag{A3}$$

in agreement with equation (21).

References

[1] Bolton J P R and Chen M 1995 *J. Phys.: Condens. Matter* 7 3373
[2] Howie A 1983 *Ultramicroscopy* **11** 141
[3] Walls M G and Howie A 1989 *Ultramicroscopy* **28** 40–2
[4] Garcia-Molina R, Gras-Marti A, Howie A and Ritchie R H 1985 *J. Phys. C: Solid State Phys.* **18** 5335–45
[5] Parker A 1988 Part 2 project, University of Cambridge
[6] Walsh C A Private communication
[7] Chen M 1994 Applications of computer algebra to the theory of electron energy loss *PhD Thesis* Open University
[8] Bolton J P R and Chen M 1994 Dispersion brackets and electron energy loss *Open University Technical Report*
[9] Ritchie R H and Eldridge H B 1962 *Phys. Rev.* **126** 1935–47
[10] Seely S and Poularikas A D 1979 *Electromagnetics* (New York: Decker)
[11] Landau L D and Lifshitz E M 1960 *Electrodynamics of Continuous Media* (New York: Pergamon)
[12] Economou E N 1969 *Phys. Rev.* B **182** 539–54
[13] Palik E D 1985 *Handbook of Optical Constants of Solids* (New York: Academic)